THE JOURNAL OF
PHYSICAL CHEMISTRY C

Article

pubs.acs.org/JPCC

Thermochemical Behavior of Nickel-Coated Nanoaluminum Particles

Dilip S. Sundaram, Puneesh Puri,† and Vigor Yang*

School of Aerospace Engineering, Georgia Institute of Technology, Atlanta, Georgia 30332, United States

Supporting Information

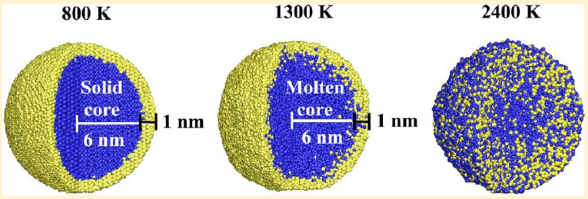

ABSTRACT: Thermochemical behavior of nickel-coated aluminum particles in the size range of 4−18 nm is studied using molecular dynamics simulations. The analysis is carried out in isothermal−isobaric and isochoric-isoenergetic ensembles using an embedded atom method. Emphasis is placed on analyzing the melting points of the core and shell, diffusion of atoms, and intermetallic reactions. The aluminum core melts at a temperature greater than the melting point of a nascent aluminum particle due to the cage-like mechanical constraint imposed by the nickel shell. The melting point of the aluminum core increases from 775 to 1000 K when the core diameter increases from 3 to 12 nm. The melting point of the core is not significantly affected by variations in the shell thickness in the range of 1−3 nm, although the melting point of the shell increases with increasing thickness from a value as low as 1100 K at 1 nm to 1580 K at 3 nm. Melting is followed by diffusion of atoms and energy release due to intermetallic reactions, which result in ignition of the particle in vacuum. For a core diameter of 3 nm, the ignition temperature increases from 800 to 1600 K when the shell thickness increases from 0.5 to 3.0 nm. The diffusion coefficient of aluminum atoms in the nickel shell exhibits an exponential dependence on temperature, with activation energy of 34.7 kJ/mol. The adiabatic reaction temperature of the particle increases from 1650 to 2338 K when the core diameter increases from 3 to 8 nm. The calculated values agree reasonably well with those obtained via thermodynamic energy balance analysis.

I. INTRODUCTION

Aluminum particles are extensively used in many propulsion and energy-conversion applications due to their favorable energetic properties.[1] They are covered by an amorphous oxide layer, which is typically 0.5−4 nm thick.[2] The specific thickness of the oxide layer depends on the temperature of the particle and the duration of exposure to the oxidizing environment. When the particle is exposed to the oxidizing gas for a sufficient period, the oxide layer thickness saturates at a value of 4 nm.[3] The oxide layer protects the particle from further attack by the oxidizer molecules. Aluminum particles with diameter greater than 100 μm ignite only upon melting of the oxide layer at 2350 K.[4] This results in a long ignition delay and a slow rate of energy release. It is thus desirable to reduce the ignition temperature of micrometer-sized aluminum particles.

The formation of the oxide layer on aluminum particles can be significantly inhibited by applying transition metal coatings, which have higher melting points than the aluminum.[5] For example, the bulk melting point of nickel is 1728 K. Foley et al.[5] synthesized nanoaluminum powders by thermal decomposition of an alane-adduct solution in the presence of a titanium catalyst under an inert atmosphere. The resulting material was used to reduce complexes of gold, nickel, palladium, and silver. The reduction process yielded nanoaluminum particles coated with transition metals. Typically, an oxide layer of the transition metal is formed, which can have thickness on the order of few nanometers.[5,6] Among all transition metals considered in Foley et al.'s study, nickel resulted in the highest active aluminum content. Encapsulation of aluminum particles with a nickel shell results in lower ignition temperatures due to intermetallic reactions between aluminum and nickel atoms.[7] For example, the ignition temperature of a 2.38 mm aluminum particle in air decreases from 2350 to 1313 K when the oxide layer is replaced with a nickel coating. Temperature runaway is also observed in inert environments.[7] The substitution of a nickel coating for the oxide coating increases the flame speed of an aluminum particle dust in air by a factor of 1.5−4.[8] Nickel-coated aluminum particles can potentially be employed to manufacture nickel aluminides (Ni_xAl_{1-x}), which are attractive for use in aircraft turbines due to their good strength characteristics, excellent corrosion and oxidation resistance, and high melting points.[9] A better understanding of its thermochemical behavior is thus helpful for propulsion and material synthesis applications.

Nanosized particles have unusual energetic properties due to their high percentage of surface atoms and the excess energy associated with these atoms.[10−12] As the particle size decreases from 30 to 3 nm, the percentage of surface atoms increases from 5 to 50%.[13] The melting temperature of a nanoaluminum particle increases from 473 K at 2 nm to a bulk value of 937 K at ∼8 nm.[14] The ignition temperature can be as low as 933 K, possibly due to polymorphic phase transformations in the oxide layer or melting of the aluminum core.[2,15] The oxide layer, however, occupies a significant portion of the particle mass on nanoscales. For example, a 38 nm aluminum particle has ∼47.5 wt % oxide.[16] For combustion applications, therefore, it is

Received: December 17, 2012
Revised: February 8, 2013
Published: March 27, 2013

dx.doi.org/10.1021/jp312436j | J. Phys. Chem. C 2013, 117, 7858−7869

desirable to replace the oxide coating with such favorable metallic coatings as nickel. Nickel atoms can participate in oxidation and intermetallic reactions, thereby resulting in a significant reduction in the ignition delay.

Molecular dynamics (MD) simulations can be used to provide insight into the melting and ignition characteristics of nanoscale materials. Puri and Yang[14] performed MD simulations to analyze the effect of particle size on melting of nascent aluminum particles. The thermomechanical behavior of oxide-coated aluminum particles has also been analyzed.[17] MD simulations on nickel-coated aluminum particles have thus far, however, been limited. Most efforts were made to study the possibility of fragmentation of the shell caused by core melting at a fixed core/particle size,[18,19] with little attention paid to diffusion and intermetallic reactions.[19,20] Systematic studies of the effect of particle size on the physiochemical processes after melting of the core are yet to be performed. In the present study, the thermochemical behavior of nickel-coated aluminum particles is investigated via MD simulations over a wide range of temperatures to characterize melting, diffusion, and intermetallic reactions. The core diameter of the particles of interest is in the range of 3−12 nm, and shell thicknesses of 0.5, 1, 2, and 3 nm are considered. Special attention is paid to quantify the effects of the core diameter and shell thickness on relevant physiochemical phenomena.

II. THEORETICAL AND COMPUTATIONAL FRAMEWORK

In the present study, both isobaric−isothermal (NPT) and isochoric-isoenergetic (NVE) ensembles are employed. NPT ensemble is used to study the thermochemical behavior of the particle in the presence of external heating at a constant pressure condition, while NVE ensemble is used to investigate self-heating of the particle due to intermetallic reactions under adiabatic conditions. In NPT ensemble, a system of N atoms is coupled to an external source by introducing additional variables into the Lagrangian. Assuming that atoms behave as classical point-like masses, the Lagrangian, L, is expressed as

$$L_{\mathrm{NPT}} = \sum_i \frac{m_i s^2 V^{2/3} \dot{q}_i^{\,2}}{2} - U(V^{1/3} q_i) + \frac{M\dot{V}^2}{2} - PV + \frac{Q\dot{s}^2}{2} \text{-} g k_{\mathrm{B}} T \ln s \tag{1}$$

where M is a constant fictitious mass associated with the volume of the system, m is the mass of the atom, q_i is the generalized coordinate, V is the volume, treated as a dynamic variable, P is the pressure, U is the potential energy, T is the temperature, Q is the inertia factor, g is a parameter, k_{B} is the Boltzmann constant, and s is the degree of freedom of the thermostat. In this method, volume is treated as a dynamic variable[21] and the parameter s controls heat exchange between the system and the reservoir.[22] Substituting the Lagrangian in the Euler−Lagrange equation,[23] the equations of motion take the form

$$\begin{aligned} M\ddot{V} &= -P + \frac{s^2}{3V}\Big[V^{2/3}\sum_i m_i \dot{q}_i^{\,2} - V^{1/3}\sum_i F_i q_i\Big] \\ m_i \ddot{q}_i &= \frac{V^{-1/3} F_i}{s^2} - \frac{2 m_i \dot{V} \dot{q}_i}{3V} - \frac{2 m_i \dot{s} \dot{q}_i}{s} \\ Q\ddot{s} &= s V^{2/3} \sum_i m_i \dot{q}_i^{\,2} - \frac{g k_{\mathrm{B}} T}{s} \end{aligned} \tag{2}$$

where $\dot{q}_i$ and $\ddot{q}_i$ denote the first-order and second-order derivatives of q_i with respect to time and F_i is the net force on atom i. In the NVE ensemble, the Lagrangian is the difference between the kinetic and potential energies of the set of atoms. The resulting equation of motion is given by

$$m_i \ddot{q}_i = -\frac{\partial U}{\partial q_i} \tag{3}$$

The above system of equations is numerically integrated using a fifth-order predictor−corrector algorithm. The time step is chosen as 1 fs because the time scale of vibration of atoms is on the same order. Negligible improvement in the model results is obtained when the time step is reduced from 1 to 0.1 fs. The heating rate is another important adjustable parameter. Shibuta and Suzuki[24] analyzed the effect of the cooling rate on the solidification of metal nanoparticles using MD simulations. The solidification temperature decreased with increasing cooling rate. In the present work, a parametric study was conducted to determine the optimum value of the heating rate in the range 10^{-3} to 10^{-1} K/fs. The result is shown in Figure 1. The time step places restriction on the minimum value of the heating rate. The analysis reveals that a heating rate lower than 10^{-2} K/fs increases the total computational time dramatically with only little change in the model results, while a higher value leads to substantially different results. As a result, a heating rate of 10^{-2} K/fs is adopted in the present study.

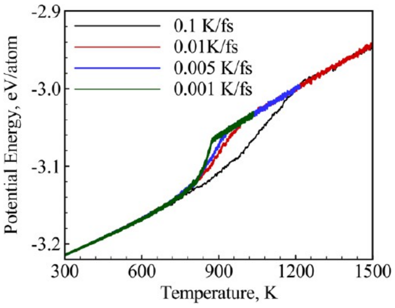

Figure 1. Variation of potential energy of 7 nm (10976 atoms) aluminum particle with temperature at different heating rates.

To calculate macroscopic properties of the system from the positions and momenta of all atoms, an ensemble average is required.[23] The pressure is calculated using the virial equation of state as a function of temperature and forces experienced by all of the atoms.[25]

$$P = N k_{\mathrm{B}} T + \left\langle \frac{1}{3} \sum_{i=1}^{N} r_i \cdot F_i \right\rangle \tag{4}$$

where r_i is the position vector of atom i. The melting point of the system is identified based on the variations in the potential energy, Lindemann index, thermal displacement, and translational-order parameter. The Lindemann index, δ, is a measure of the root-mean-square fluctuations of the interatomic distance and is given by[26]

$$\delta = \frac{2}{N(N-1)}\sum_{i<j}\frac{\sqrt{\langle r_{ij}^{2}\rangle_t - \langle r_{ij}\rangle_t^{2}}}{\langle r_{ij}\rangle_t} \tag{5}$$

It is expected to increase abruptly during melting. The translational-order parameter, λ, is expressed as[27]

$$\lambda = \frac{1}{N}\sqrt{\left(\sum_{i=1}^{N}\cos(k\cdot r_i)\right)^2 + \left(\sum_{i=1}^{N}\sin(k\cdot r_i)\right)^2}$$

$$k = \left(\frac{(2N)^{1/3}\pi}{L}\right)(-1,\ 1,\ 1) \tag{6}$$

where k is an arbitrary vector of the lattice and L is the side length of the simulation domain. In solids, atoms simply translate about their lattice positions, and hence there is a perfect order in the crystal. Such order, however, disappears in a liquid state, and the corresponding translational-order parameter is reduced by an order of magnitude. The thermal displacement is defined as

$$\delta_{t,i} = \sqrt{(r_i - r_{0,i})^2} \tag{7}$$

where the subscripts i and 0 refer to atom i and the initial state, respectively. Upon melting, the aluminum atoms diffuse into the nickel shell. The onset of diffusion is marked by the sudden increase in the core radius, r_c[18]

$$r_c = \sqrt{\frac{5}{3N}\sum_{i=1}^{N_{Al}}(r_i - r_{cm})^2} \tag{8}$$

where r_{cm} is the position vector of the center of mass.

III. POTENTIAL FUNCTION

To close the formulation, the potential energy of the system of atoms needs to be specified. For metals, the majority of the potential functions are based on the embedded atom method.[28] In this method, the energy needed to embed an atom in the electron gas is included to capture the physics of metallic bonding. One such potential function, which is formulated by Cleri and Rosato,[29] has been fitted to the structural and thermodynamic properties of bulk aluminum and nickel. It takes the following form:

$$U = \sum_{i=1}^{N}\left(\sum_{j\neq i}V_{ij} - \sqrt{\sum_{j}\rho_{ij}}\right) \tag{9}$$

where V is the pair-potential function and ρ is the electron density function. The first term describes the electrostatic interactions between the atoms, while the second term accounts for the energy needed to embed an atom in the electron gas. The pair-potential and electron density functions are expressed as

$$V_{ij} = A_{\alpha\beta}\exp\left(-p_{\alpha\beta}\left(\frac{r_{ij}}{r_{\alpha\beta}^{0}} - 1\right)\right)$$

$$\rho_{ij} = \xi_{\alpha\beta}^{2}\exp\left(-2q_{\alpha\beta}\left(\frac{r_{ij}}{r_{\alpha\beta}^{0}} - 1\right)\right) \tag{10}$$

The parameters in the potential function are given in Table 1.[30,31] Previous studies (see refs 1−7 in the Supporting Information) indicate that the potential function can predict the structure, phase stability, and thermodynamic properties of Ni−Al alloys (especially, B2-NiAl and Ni_3Al) with reasonable accuracy. Furthermore, considerable success has been achieved in simulations of thermal behaviors of aluminum particles coated with Ni and Ni_3Al using this potential function (see refs 8 and 9 in the Supporting Information). As a result, it is employed in the present study.

Table 1. Parameters for Potential Function[30,31]

	Ni−Ni	Al−Al	Ni−Al
A (eV)	0.0376	0.1221	0.0597
ξ (eV)	1.0700	1.3160	1.2898
p	16.9990	8.6120	15.714
q	1.1890	2.5160	1.1550
r_0 (Å)	2.4910	2.8637	2.5001

IV. PURE ALUMINUM AND NICKEL

The theoretical framework is employed to calculate the structural and thermodynamic properties of aluminum and nickel. An FCC lattice is adopted to calculate the initial position vectors for a known number of atoms. For bulk materials, a periodic boundary condition is enforced in all three spatial directions. A free-surface boundary condition is, however, prescribed for nanoparticles. The crystal is allowed to equilibrate at 300 K prior to the heating simulation.

A. Bulk Materials. The properties of surface-free bulk systems of aluminum and nickel are first treated. The lattice constant and cohesive energy are calculated by equilibrating the crystal in an NVE ensemble. To determine the melting point and latent heat of melting, the crystal is heated externally in an NPT ensemble. Table 2 shows calculated values of the cohesive energy, lattice constant, and latent heat of melting and compares them with experimental data. The discrepancy is <2%, demonstrating the accuracy of the potential function. Figure 2 shows the melting of 4000-atom bulk aluminum in vacuum. Melting is observed at 1060 K, at which point sharp variations occur in the translational-order parameter and Lindemann index. Such a trend is characteristic of the structural melting phenomenon, which is observed for surface-free materials.[35] Note that the fluctuations that are typically

Table 2. Cohesive Energy, Lattice Constant, and Latent Heat of Melting of Bulk Materials

	aluminum		nickel	
	model	experiment[32−34]	model	experiment[32−34]
E_c (eV/atom)	−3.337	−3.340	−4.437	−4.435
a (Å)	4.048	4.050	3.491	3.520
ΔH_m (kJ/mol)	10.610	10.470	17.360	17.160

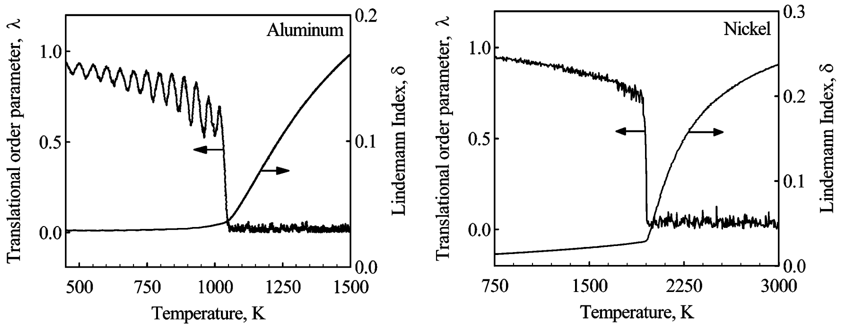

Figure 2. Translational order parameter (λ) and Lindemann index (δ) as a function of temperature showing the melting of bulk aluminum and nickel in vacuum.

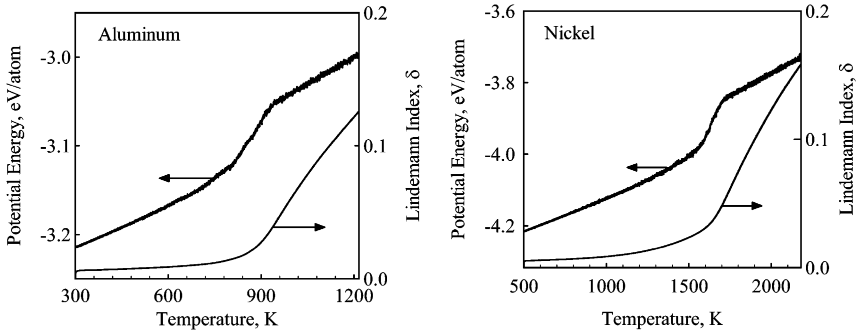

Figure 3. Potential energy and Lindemann index (δ) as a function of temperature showing the melting of 10 976-atom aluminum (7 nm) and nickel (6 nm) particles in vacuum.

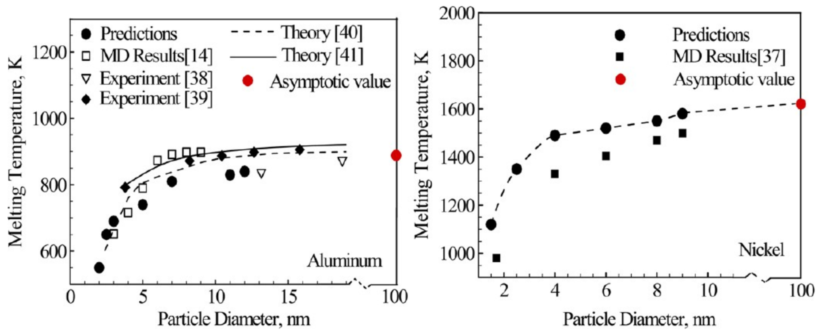

Figure 4. Effect of particle size on melting of aluminum and nickel particles.

observed in MD simulations decrease with increasing number of atoms. The system is superheated above the experimental melting point of bulk material by 127 K, which can be attributed to the absence of a nucleation site for melting. The structural melting point is typically greater than the thermodynamic counterpart by 20%.[35,36] The resulting asymptotic value of the melting temperature of aluminum particles is 883 K, which differs from the experimental value by ~5%. A similar pattern is observed for bulk nickel, as shown in Figure 2. It melts at 1950 K, which is higher than the thermodynamic melting point by 222 K. The asymptotic heterogeneous melting point of 1625 K is 6% lower than the experimental value.

B. Nascent Nanoparticles. The melting of nanoscale particles is examined over a size range of 1.5−12 nm. Figure 3 shows the variation with temperature of the potential energy and Lindemann index of a 7 nm aluminum particle consisting of 10 976 atoms. Melting occurs at 810 K. For a particle, the surface acts as a nucleation site for phase transition and the melting front propagates to the interior regions of the core. Hence, the phase change is manifested by a gradual increase in the properties, as opposed to the abrupt changes found in a bulk material. A similar trend is observed for the nickel particle, except that melting takes place at a higher temperature of 1540 K. Figure 4 shows the effect of particle size on the melting of aluminum and nickel on nanoscales. It also shows comparison with the results of previous MD simulations,[14,37] experiments,[38,39] and theoretical studies.[40,41] The theoretical curve in ref 40. corresponds to the case in which only the Ginzburg−Landau (GL) equation is employed. For nanosized particles, surface premelting phenomenon is observed. Because the percentage of surface atoms increases with decreasing particle size, a larger particle melts at a higher temperature. Note that the dependence of the melting point on particle size becomes much weaker for diameters greater than 5 nm. Eckert et al.[38] synthesized nanocrystalline aluminum powders by mechanical attrition in argon, hydrogen, and oxygen atmospheres. A similar reduction was observed in the melting point with decreasing grain size. It is rather surprising that the predicted values exhibit excellent agreement with experimental data because the model underpredicts the bulk melting point by 5%. This may be attributed to the fact that the heating rates in the simulations are orders of magnitude higher than those employed in the experiments.[42] Furthermore, the theoretical and experimental melting points increase more gradually than those in MD simulations. This is completely justified because the percentage of surface atoms in the particle follows a similar trend. Qi et al.[37] calculated the melting points of nickel particles as a function of particle size using the quantum-corrected Sutton−Chen potential. As can be seen, the Cleri−Rosato potential function offers more accurate values of the melting point of nickel particles.

V. NICKEL-COATED ALUMINUM PARTICLES

The theoretical model is also employed to analyze the thermochemical behavior of nickel-coated aluminum particles. Figure 5 shows the initial structure of nickel-coated aluminum particle with a core diameter of 12 nm and shell thickness of 1 nm. A spherical nickel particle of known dimension is first generated. A spherical void is then created in the interior of the nickel particle to accommodate the aluminum core. The resulting particle is equilibrated at 300 K prior to the heating simulation. Table 3 shows the values of the core diameter (d_c), shell thickness (δ_s), total number of atoms (N), and number of aluminum atoms (N_{Al}). The core diameter varies in the range of 3−12 nm, and three different shell thickness of 0.5, 1, 2, and 3 nm are considered. The aluminum atomic fraction increases with increasing core size and decreasing shell thickness.

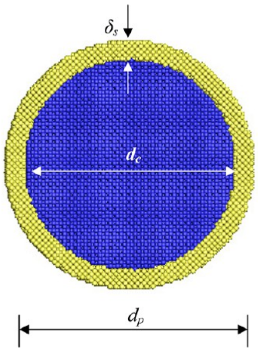

Figure 5. Initial crystal structure of nickel-coated aluminum particle ($d_p = d_c + 2\delta_s$).

Table 3. Configuration of Nickel-Coated Nanoaluminum Particles

d_c, nm	δ_s, nm	N	N_{Al}	X_{Al}
3	0.5	2909	874	0.30
3	1.0	7187	874	0.12
3	2.0	17 440	874	0.05
3	3.0	37 065	874	0.02
5	1.0	15 496	4081	0.26
6	1.0	20 914	6380	0.30
6	0.5	12 760	6380	0.50
8	1.0	39 435	15 504	0.39
12	1.0	103 737	53 752	0.52
12	2.0	169 899	53 752	0.31
12	3.0	254 614	53 752	0.21

A. Baseline Simulation. To facilitate detailed discussion on the thermochemical behavior of nickel-coated aluminum particles, we first consider a particle with a core diameter of 12 nm and shell thickness of 1 nm. Figure 6 shows the variation of the Lindemann index and potential energy of the core with temperature. Melting of the core is characterized by the change in the parameters, beginning at 1000 K. The predicted melting point is higher than that of a nascent particle, which is ∼880 K. It is, however, lower than the structural melting point of bulk aluminum, 1060 K. The latter represents the upper limit for the core melting point because it is the temperature at which the crystal undergoes catastrophic mechanical failure. The melting point elevation for a coated nanoparticle has been observed in previous experimental[36,43−46] and theoretical[47,48] studies. The enhanced thermal stability of an encapsulated core is attributed to the epitaxial core−shell interface or to the pressure buildup. The former is present in the particles considered in the present study, as seen in Figure 5. In an uncoated particle, the surface atoms, which have higher energy than the atoms in the interior region, can vibrate easily. For a coated particle, the shell restricts the vibration of the interfacial core atoms, which have lower energy than those in the interior region. As a result, a significant increase in the melting point is observed.

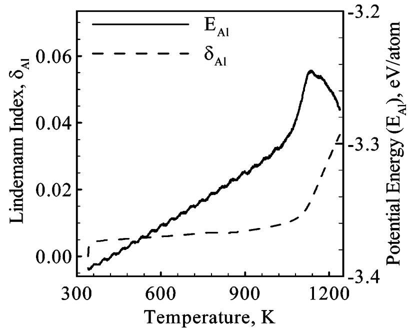

Figure 6. Lindemann index, δ_{Al}, and potential energy of the aluminum core as a function of temperature for a 14 nm particle with a 1 nm thick nickel shell.

Figure 7 shows the snapshots of the particle at 300 and 1100 K. Melting causes a significant change in the crystal structure of the core. At 300 K, a well-defined structural order is present, but no such order is observed at 1100 K. The crystal structure of the shell is negligibly affected. Figure 8 shows the variation of the core radius with temperature. The sudden increase in the core radius at ∼1000 K may be attributed to the volume dilation of the core associated with melting. Note that the aluminum core dissolves nickel atoms at the interface. The aluminum atoms continue to diffuse into the shell, which causes the core radius to increase monotonically. Figure 9 shows the diffusion processes occurring in the particle over the temperature range of interest (300−2400 K). Aluminum atoms diffuse into the shell and nickel atoms diffuse into the core, resulting in the formation of a homogeneous alloyed particle. The diffusion processes prevail upon melting due to the higher mobility of the melted atoms. Note that complete homogenization is not observed at 2400 K, suggesting that higher temperatures are required for complete mixing of the core and shell atoms. Figure 10 shows the variation of the average potential energy of the particle with temperature. The potential energy rises, attains a plateau, and then decreases. This trend is a characteristic of the core−shell particle structure and is not observed for nascent

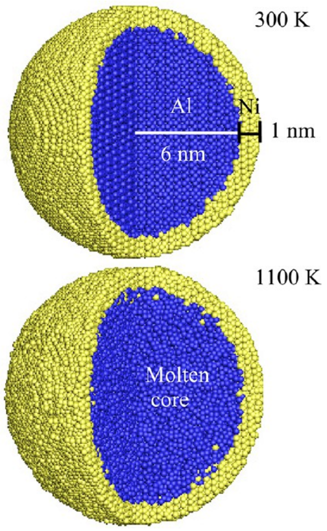

Figure 7. Snapshot of the particle before (300 K) and after (1100 K) core melting.

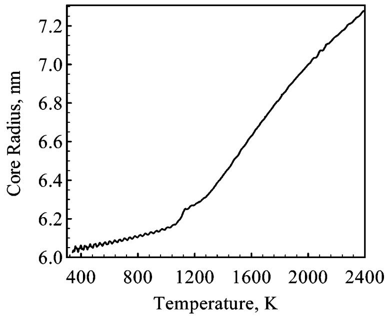

Figure 8. Core radius as a function of temperature for 14 nm particle with a 1 nm thick Ni shell.

particles. The result suggests the formation of low-energy species from the following exothermic intermetallic reaction:

$$\mathrm{Ni} + \mathrm{Al} \rightarrow \mathrm{NiAl} \qquad (11)$$

The heat of formation of NiAl is 62 kJ/mol at room temperature.[49] The initial rise in the potential energy is caused by the transfer of energy from the heat reservoir to the particle. The plateau represents the stage in which this energy supply is counterbalanced by the formation of the low-energy species, NiAl. The subsequent decrease indicates the preponderance of the intermetallic reactions.

Note that the interfacial aluminum atoms mix with nickel atoms even at room temperature. If the particle is heated externally to a temperature at which the reactions begin to occur rapidly, it can ignite, provided that the rate of chemical heat generation is greater than that of heat loss to the ambient environment. An energy balance is performed to estimate the equilibrium temperature of the particle upon completion of the intermetallic reactions under adiabatic conditions. The result is compared with the value obtained from the MD simulation. The thermodynamic energy balance takes the form

$$H_{\mathrm{reac}}(T_{\mathrm{i}}) = H_{\mathrm{prod}}(T_{\mathrm{ad}}) \qquad (12)$$

where H_{reac} is the enthalpy of the reactants calculated at an initial temperature, T_{i}, and H_{prod} is the enthalpy of the products evaluated at the adiabatic reaction temperature, T_{ad}. The initial temperature is taken as 1250 K, which corresponds to the point at which the potential energy begins to decrease. The enthalpy of the reactants, H_{reac}, is given by

$$H_{\mathrm{reac}} = H_{\mathrm{Al}}^{1250\mathrm{K}} + H_{\mathrm{Ni}}^{1250\mathrm{K}} + H_{\mathrm{m,Al}} \qquad (13)$$

The enthalpies of Al and Ni are calculated as 22.85 and 24.82 kJ/mol, respectively, and that of the melting of aluminum is taken as 10.71 kJ/mol. The enthalpy of the products is expressed as

$$H_{\mathrm{prod}} = \left(1 - \frac{t_{\mathrm{i}}A}{V}\right) H_{\mathrm{f,NiAl}}^{298\mathrm{K}} + C_{p,\mathrm{NiAl}}(T_{\mathrm{ad}} - 298) + H_{\mathrm{m,NiAl}} \qquad (14)$$

where A is the interfacial area, V is the core volume, and t_{i} the thickness of the interfacial zone. The interfacial core atoms participate in alloying reactions prior to melting of the core, thereby resulting in a decrease in the energy content of the particle. The fraction of the core volume that has already

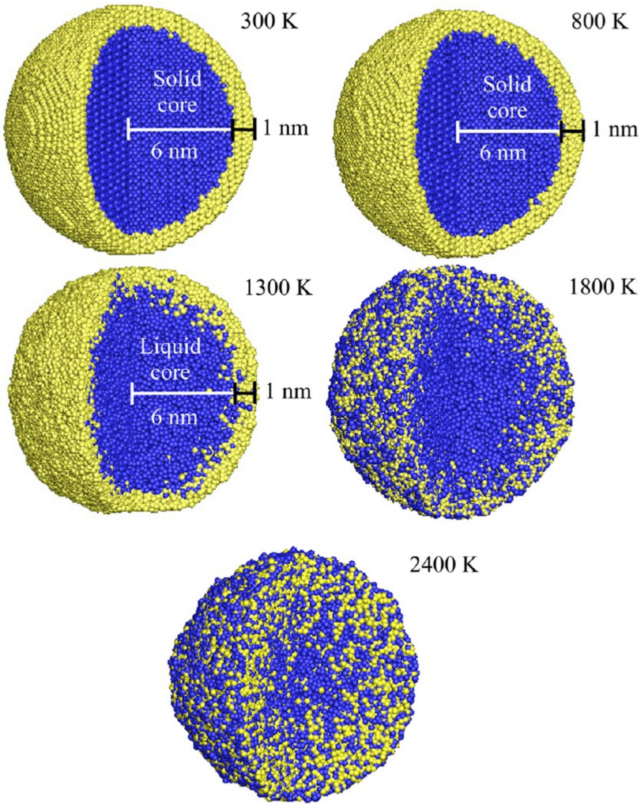

Figure 9. Snapshots of 14 nm particle showing melting and diffusion processes.

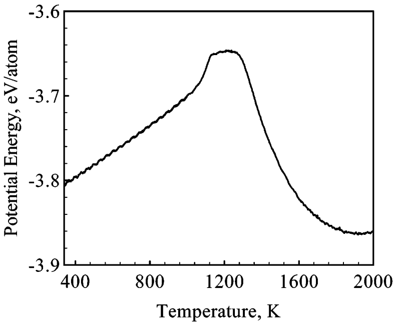

Figure 10. Average potential energy of the particle as a function of temperature for core diameter of 12 nm and shell thickness of 1 nm.

reacted depends on the interfacial area-to-core volume ratio and the thickness of the interfacial zone. The latter is approximated to be 0.7 Å.[19] The specific heat and enthalpy of melting of NiAl are taken as 55 J/mol-K and 63 kJ/mol, respectively.[50] The equilibrium temperature calculated using eqs 13 and 14 is 2388 K. In other words, the particle is self-heated from 1250 to 2388 K due to the heat release from intermetallic reactions.

Figure 11 shows the variation of the temperature of the particle with time under adiabatic conditions calculated using MD simulations. The initial position and velocities of atoms are those obtained from the heating simulation in an NPT ensemble at 1250 K. The particle is heated from 1250 to ~2300 K due to exothermic intermetallic reactions of aluminum and nickel atoms over a period of 100 ps. One of the reasons for the discrepancy is that equilibrium is not attained within a time period of ~100 ps. After a time period of 50 ps, the temperature increases very slowly. The particle snapshots obtained in NPT simulations also support this argument. It is also important to note that the atomic species are no longer expected to interact with a ground electronic configuration but with an excited one at higher temperatures. Therefore, classical many-body potentials reproduce interaction forces only with modest accuracy, and ab initio methods should be applied. Note that the particle temperature increases by ~1000 K over a time period of ~100 ps. The resulting intrinsic heating rate is ~10^{13} K/s, which is equivalent to particle ignition.

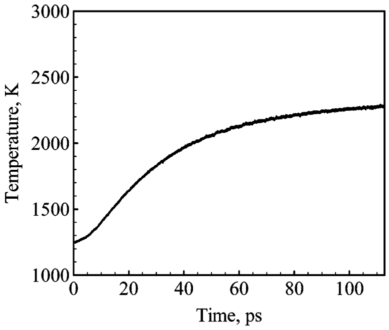

Figure 11. Temporal evolution of the particle temperature for core diameter of 12 and 1 nm thick shell.

B. Effect of Core Size. The effect of core size is studied in the diameter range of 3−12 nm with a fixed shell thickness of 1 nm. Figure 12 shows the variation of the melting point of the core with the core diameter. It increases from 775 to 1000 K when the core diameter increases from 3 to 12 nm. Such a trend has also been observed in a previous study.[17] In all of the cases, the presence of the nickel shell increases the melting point of the core. Figure 13 shows the snapshots of an 8 nm particle colored by thermal displacement at different temperatures. As can be seen, the nucleation of the liquid phase begins at the core−shell interface, and the melting front propagates to the interior region of the core. The fact that heterogeneous nucleation at the interface dominates melting of superheated nanoparticles has been observed previously in MD simulations.[47]

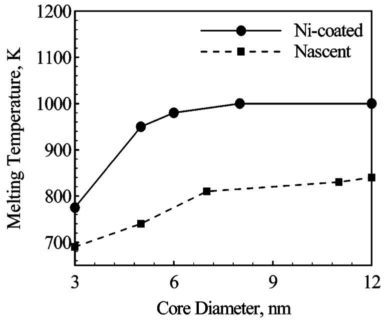

Figure 12. Effect of core diameter on the melting point of the core for a shell thickness of 1 nm.

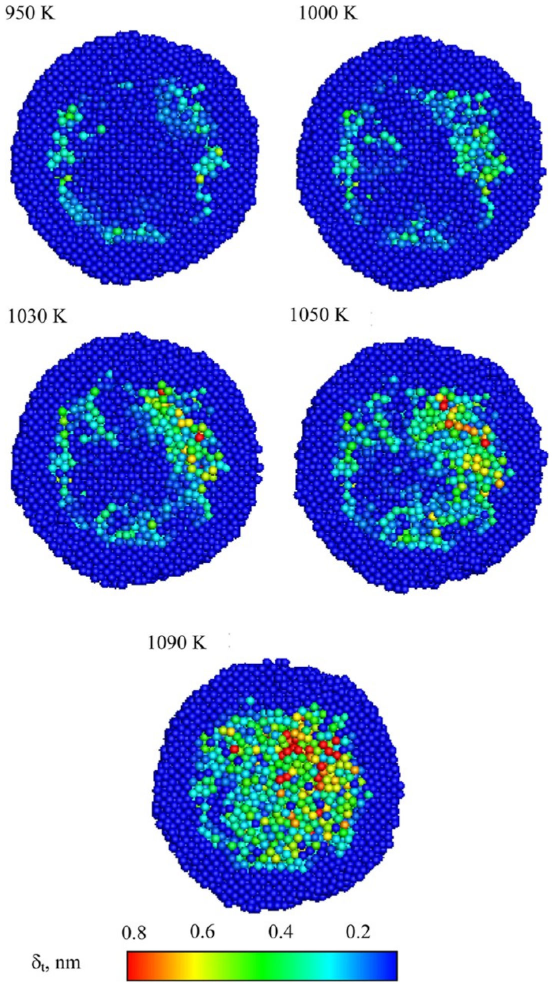

Figure 13. Particle snapshots showing thermal displacement of core atoms at different temperatures for 8 nm particle with 1 nm shell.

Figure 14 shows the variation of the core radius with temperature for different core sizes. For a 3 nm core, the diffusion rate of aluminum atoms increases suddenly at 1350 K, a phenomenon that is not related to the melting of the core. The nickel shell melts at 1325 K (see Section V.C), which is lower than the bulk melting point of nickel, 1728 K. Unlike a particle, a shell can begin to melt both at the surface and at the core−shell interface. The nickel shell with a molten aluminum cluster is less stable than a pure nickel particle of the same size.[36] For larger core diameters, the aluminum atoms begin to diffuse outward at slightly lower temperatures. Figure 15 shows the variation of the average potential energy of the particle with temperature. The magnitude by which the potential energy decreases is proportional to the core size. In other words, the smaller the core, the lower the chemical heat release due to the

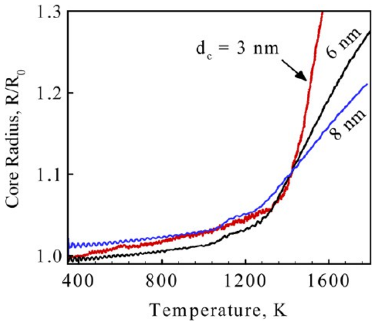

Figure 14. Normalized core radius as a function temperature for shell thickness of 1 nm.

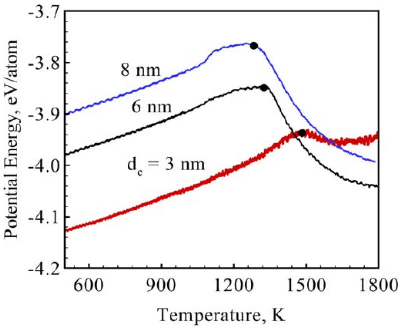

Figure 15. Effect of core diameter on the potential energy for a shell thickness of 1 nm.

intermetallic reactions. The temperature at which the core radius begins to increase suddenly may be identified as the ignition temperature. The calculated values are in the range of 1240−1350 K, which are near the melting point of the shell.

Simulations in NVE ensembles are performed to calculate the equilibrium temperature of the particle upon completion of the intermetallic reactions for different core sizes. Figure 16 shows the effect of core diameter on the adiabatic reaction temperature of the particle. At a fixed shell thickness, the reaction temperature decreases with decreasing core size. For smaller cores, the temperature increase due to the intermetallic reactions is relatively low. (For example, see Supporting Information, Figure S1.) To understand the relevant physiochemical phenomena, we also perform a companion thermodynamic analysis, and the result is included in the Figure.

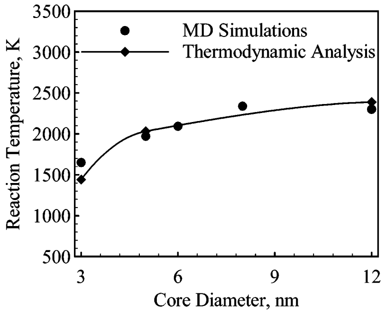

Figure 16. Effect of core diameter on adiabatic reaction temperature for 1 nm thick shell.

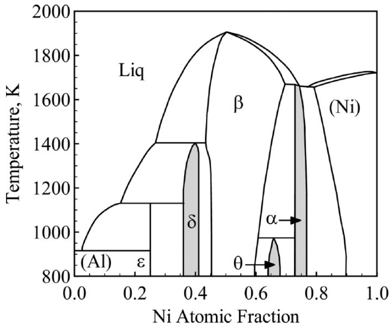

Figure 17. Ni−Al phase diagram (ε: $NiAl_3$, δ: Ni_2Al_3, β: NiAl, θ: Ni_5Al_3, and α: Ni_3Al).[51]

Figure 17 shows the equilibrium phase diagram for the Ni−Al system. The particle composition determines the intermetallic compounds that are formed. For a 3 nm core, the aluminum atomic fraction is 0.12 (nickel-rich). The resulting product is a mixture of Ni_3Al and Ni. For this case, the chemical reaction can be expressed as

$$7.2Ni + Al \rightarrow Ni_3Al + 4.2Ni \tag{15}$$

In the present analysis, the specific heat, enthalpy of fusion, and heat of formation of Ni_3Al are taken to be 130 J/mol-K, 50 kJ/mol, and −164 kJ/mol, respectively.[52] The results support the fact that the adiabatic reaction temperature decreases with decreasing core size. This can be attributed to the following reasons. First, residual Ni atoms remain in the products, which do not participate in the reactions. Second, although the interfacial zone thickness is held constant, the fraction of interfacial core atoms increases with decreasing particle size. As a result, a greater percentage of core atoms have already reacted for a smaller core. Such an effect was also observed for aluminum-coated nickel particles.[19] For the aluminum-rich particle, intermetallic compounds such as $NiAl_3$ are formed. The situation is typically encountered for aluminum-coated nickel particles. The ensuing thermal behavior is expected to be different.

C. Effect of Shell Thickness. The effect of shell thickness is examined in the range of 0.5−3.0 nm. Figure 18 shows the melting point of the aluminum core as a function of shell thickness. The core melting point is not significantly affected by variations in the shell thickness in the size range of concern. (For an illustration, see the Supporting Information, Figure S2.) Calculations indicate that the core is under compression (positive pressure on the order of 1000 MPa) and the shell is under tension. A similar trend was also obtained for homogeneously heated oxide-coated aluminum particles.[53]

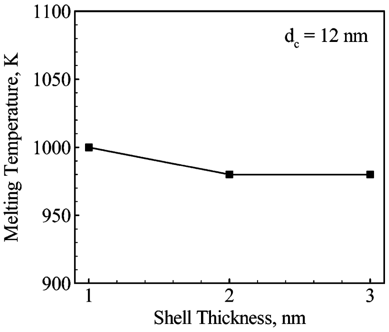

Figure 18. Effect of shell thickness on the melting temperature of the 12 nm core.

Levitas[54] proposed a melt-dispersion mechanism, which is valid at very high heating rates (>10^6 K/s). According to this theory, the shell is ruptured by the tensile stress exerted by the core and the molten aluminum clusters are dispersed in the surrounding environment. In the present study, melt dispersion is not observed, thereby suggesting that the stresses are relaxed. One possible mechanism for such a phenomenon is the diffusion of aluminum atoms. Previous studies[55,56] indicate that the independence of melting temperature with shell thickness results from stress relaxation. It is thus not surprising that the melt-dispersion mechanism is not observed for nickel-coated aluminum particles. Figure 19 shows the core radius as a function of temperature for a core diameter of 3 nm and shell thickness of 0.5, 1, 2, and 3 nm. Diffusion is facilitated for thinner shells. For a 0.5 nm shell, the core radius increases significantly upon melting of the core at 800 K. The core atoms, however, begin to diffuse out only at 1400, 1500, and 1600 K for shell thickness of 1, 2, and 3 nm, respectively. For a core diameter of 3 nm, the results suggest that the ignition temperature increases from 800 to 1600 K when the shell thickness increases from 0.5 to 3.0 nm. Figure 20 shows the effect of shell thickness on the melting point of the shell for core diameters of 3 and 12 nm. The shell melting point increases from a value as low as 1100 to 1580 K, when the thickness increases from 1 to 3 nm. In all cases, the melting point of the shell is lower than that corresponding bulk value of 1728 K. (For illustration, see the Supporting Information, Figure S3.) It is obvious that shell melting plays an important role in dictating the diffusion and ignition in nickel-coated aluminum particles.

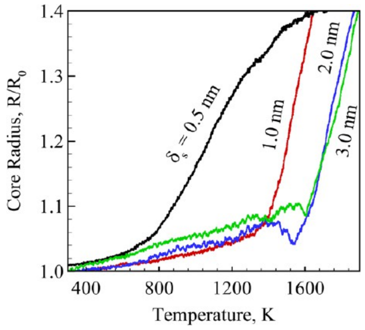

Figure 19. Variation of the core radius with temperature for a core diameter of 3 nm and shell thickness in the range of 0.5−3 nm.

The case of a particle covered by a very thin shell is of interest because a previous study indicates the possibility of ignition near room temperature.[20] Furthermore, it is possible to create a particle with a reasonably large core size and a thin shell that features an equal number of Al and Ni atoms. As a consequence, the energetics of intermetallic reactions are easily tractable. In the present study, a 7 nm particle with a 0.5 nm shell is considered. The information about the diffusion coefficient of aluminum atoms in a nickel shell is useful, especially from the standpoint of the development of macroscale ignition and combustion models. Figure 21 shows the effect of temperature on the diffusion coefficient of aluminum atoms in a nickel shell. The diffusion process is very slow at temperatures lower than the melting point of the core. A sudden increase in the diffusion coefficient takes place after melting of the core. It exhibits a temperature dependence of the form

$$D = D_0 \exp\left(-\frac{E_A}{RT}\right) \tag{16}$$

where E_A is the activation energy and D_0 is the pre-exponential factor. The curve-fit indicates a value of 34.7 kJ/mol for the activation energy and 8.19×10^{-8} m^2/s for the pre-exponential factor. Figure 22 shows the temporal evolution of the particle under adiabatic condition. The temperature increases suddenly upon melting of the core. The intermetallic reactions result in particle heating from 300 to 1420 K. The results substantiate the fact that an aluminum particle coated by a thin nickel shell can be pyrophoric even in an inert environment.

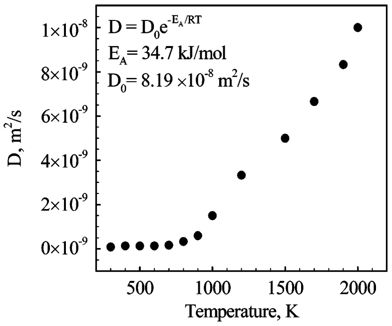

Figure 21. Diffusion coefficient of aluminum in nickel for a 7 nm particle with a 0.5 nm shell.

CONCLUSIONS

The thermochemical behavior of nickel-coated aluminum particles in the size range of 4−18 nm was studied using MD simulations. The analysis was carried out in isothermal−isobaric

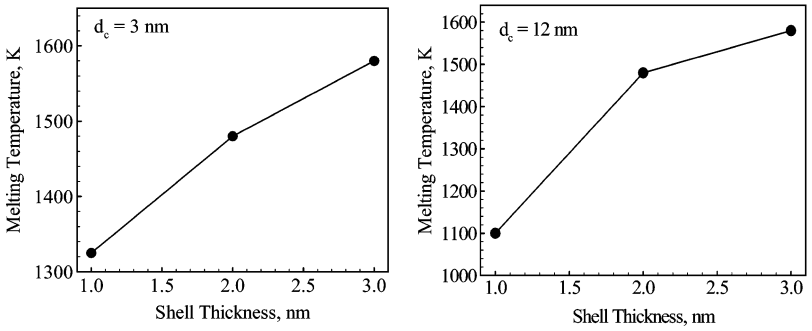

Figure 20. Effect of shell thickness on the melting temperature of the nickel shell for core diameters of 3 and 12 nm.

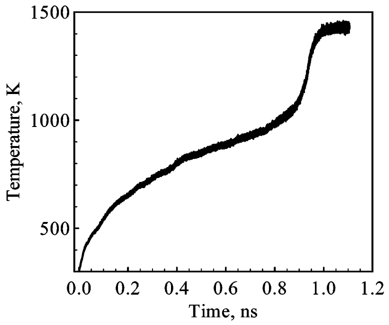

Figure 22. Temperature as a function of time for a 7 nm particle with a 0.5 nm thick shell under adiabatic condition.

and isochoric-isoenergetic ensembles using an embedded atom method. Emphasis was placed on analyzing the melting points of the core and shell, diffusion of atoms, and intermetallic reactions. The aluminum core melted at a temperature greater than the melting point of a nascent aluminum particle due to the cage-like mechanical constraint imposed by the nickel shell. The melting point of the aluminum core increased from 775 K at 3 nm to 1000 K at 12 nm. It was not significantly affected by the variations in the shell thickness in the range of 1−3 nm. The melting point of the shell increased with increasing thickness from a value as low as 1100 K at 1 nm to 1580 K at 3 nm. Melting was followed by diffusion of atoms and energy release due to intermetallic reactions, which resulted in self-heating of the particle. The diffusion coefficient of aluminum atoms in the nickel shell had an exponential dependence on temperature, with an activation energy of 34.7 kJ/mol. The adiabatic reaction temperature of the particle increased from 1650 to 2338 K when the core diameter increased from 3 to 8 nm. The calculated values exhibited reasonably good agreement with predictions from a thermodynamic energy balance analysis. The results demonstrated that nickel-coated aluminum particles can ignite even in inert environments (or in the absence of an oxidizing gas). Future work will focus on the energetics of aluminum-coated nickel particles and the comparison with the results of nickel-coated aluminum particles obtained from the present study.

■ ASSOCIATED CONTENT

Ⓢ Supporting Information

Supplementary references, variation of temperature with time in adiabatic condition for a 5 nm particle with a 1 nm thick shell, variation of the potential energy of the 12 nm core with temperature for shell thickness of 2 and 3 nm, and variation of the potential energy of the shell with temperature for a core diameter of 3 nm and shell thickness of 1, 2, and 3 nm. This material is available free of charge via the Internet at http://pubs.acs.org.

■ AUTHOR INFORMATION

Corresponding Author

*E-mail: vigor.yang@aerospace.gatech.edu. Phone: 404-894-3002. Fax: 404-894-2760.

Present Address

†Puneesh Puri: Process Technology Development Engineer, Intel, Aloha, Oregon.

Notes

The authors declare no competing financial interest.

■ ACKNOWLEDGMENTS

We thank the Air Force Office of Scientific Research (AFOSR) for their sponsorship of this program under contract no. FA9550-11-1-0002. The support and encouragement provided by Dr. Mitat Birkan is gratefully acknowledged.

■ NOMENCLATURE

a	lattice constant
A	interfacial area
Al	aluminum
C_p	specific heat
d	diameter
E_c	cohesive energy
F	force
H	enthalpy
K	kinetic energy
k	lattice vector
k_B	Boltzmann constant
L	Lagrangian, box length
m, M	mass
N	number of atoms
Ni	nickel
P	pressure
q	scaled coordinates
Q	inertia factor
r	position vector, radius
r_{ij}	interatomic distance
s	thermostat degree of freedom
T	temperature
t	time, thickness
U	potential energy
V	volume, pair potential function

Greek

ρ	electron density function
δ	Lindemann index
δ_s	shell thickness
δ_t	thermal displacement
λ	translational order parameter

Subscripts

ad	adiabatic
c	core
cm	center-of-mass
f	formation, fusion
i	initial, interface
i	atom index variable
j	atom index variable
m	melting
p	particle
prod	products
reac	reactants
t	time

■ REFERENCES

(1) Price, E. W.; Sigman, R. K. *Solid Propellant Chemistry, Combustion, and Motor Interior Ballistics*; Yang, V., Brill, T. B., Ren, W. Z., Eds.; AIAA Progress in Astronautics and Aeronautics: Reston, VA, 2000; Vol. *185*; pp 663−687.

(2) Trunov, M. A.; Schoenitz, M.; Dreizin, E. L. Effect of Polymorphic Phase Transformations in Alumina Layer on Ignition of Aluminum Particles. *Combust. Theory Modell.* **2006**, *10*, 603−623.

(3) Campbell, T.; Kalia, R. K.; Nakano, A.; Vashishta, P. Dynamics of Oxidation of Aluminum Nanoclusters using Variable Charge

Molecular-Dynamics Simulations on Parallel Computers. *Phys. Rev. Lett.* **1999**, *82*, 4866−4869.

(4) Huang, Y.; Risha, G. A.; Yang, V.; Yetter, R. A. Effect of Particle Size on Combustion of Aluminum Particle Dust in Air. *Combust. Flame* **2009**, *156*, 5−13.

(5) Foley, T. J.; Johnson, C. E.; Higa, K. T. Inhibition of Oxide Formation on Aluminum Nanoparticles by Transition Metal Coating. *Chem. Mater.* **2005**, *17*, 4086−4091.

(6) Uchikoshi, T.; Sakka, Y.; Yoshitake, M.; Yoshihara, K. A Study of the Passivating Oxide Layer on Fine Nickel Particles. *Nanostruct. Mater.* **1994**, *4*, 199−206.

(7) Shafirovich, E.; Mukasyan, A.; Thiers, L.; Varma, A.; Legrand, B.; Chauveau, C.; Gokalp, I. Ignition and Combustion of Al Particles Clad by Ni. *Combust. Sci. Technol.* **2002**, *174*, 125−140.

(8) Yagodnikov, D. A.; Voronetskii, A. V. Experimental and Theoretical Study of the Ignition and Combustion of an Aerosol of Encapsulated Aluminum Particles. *Combust., Explos. Shock Waves (Engl. Transl.)* **1997**, *33*, 49−55.

(9) Andrzejak, T. A.; Shafirovich, E.; Varma, A. Ignition Mechanism of Nickel-Coated Aluminum Particles. *Combust. Flame* **2007**, *150*, 60−70.

(10) Ilyin, A. P.; Gromov, A. A.; Vereshchagin, V. I.; Popenko, E. M.; Surgin, V. A.; Lehn, H. Combustion of Agglomerated Ultrafine Aluminum Powders in Air. *Combust., Explos. Shock Waves (Engl. Transl.)* **2001**, *37*, 664−669.

(11) Kwon, Y. S.; Gromov, A. A.; Ilyin, A. P.; Popenko, E. M.; Rim, G. H. The Mechanism of Combustion of Superfine Aluminum Powders. *Combust. Flame* **2003**, *133*, 385−391.

(12) Pivkina, A.; Ulyanov, P.; Frolov, Y.; Zavyolov, S.; Schoonman, J. Nanomaterials for Heterogeneous Combustion. *Propellants, Explos., Pyrotech.* **2004**, *29*, 39−48.

(13) Klabunde, K. J.; Stark, J.; Koper, O.; Mohs, C.; Park, D. G.; Decker, S.; Jiang, Y.; Lagadic, I.; Zhang, D. Nanocrystals as Stoichiometric Reagents with Unique Surface Chemistry. *J. Phys. Chem.* **1996**, *100*, 12142−12153.

(14) Puri, P.; Yang, V. Effect of Particle Size on Melting of Aluminum at Nano Scales. *J. Phys. Chem. C* **2007**, *111*, 11776−11783.

(15) Rai, A.; Lee, D.; Park, K.; Zachariah, M. R. Importance of Phase Change of Aluminum in Oxidation of Aluminum Nanoparticles. *J. Phys. Chem. B* **2004**, *108*, 14793−14795.

(16) Risha, G. A.; Son, S. F.; Yetter, R. A.; Yang, V.; Tappan, B. C. Combustion of Nano-Aluminum and Liquid Water. *Proc. Combust. Inst.* **2007**, *31*, 2029−2036.

(17) Puri, P.; Yang, V. Thermomechanical Behavior of Nano-aluminum Particles with Oxide Layers During Melting. *J. Nanopart. Res.* **2010**, *12*, 2989−3002.

(18) Delogu, F. Numerical Simulation of the Thermal Response of Al Core/Ni Shell Nanometer-Sized Particles. *Nanotechnology* **2007**, *18*, 505702.

(19) Henz, B. J.; Hawa, T.; Zachariah, M. Molecular Dynamics Simulation of the Energetic Reaction between Ni and Al Nano-particles. *J. Appl. Phys.* **2009**, *105*, 124310.

(20) Evteev, A. V.; Levchenko, E. V.; Riley, D. P.; Belova, I. V.; Murch, G. E. Reaction of a Ni-Coated Al Nanoparticles to Form B2-NiAl: A Molecular Dynamics Study. *Philos. Mag. Lett.* **2009**, *89*, 815−830.

(21) Andersen, H. C. Molecular Dynamics Simulations at Constant Pressure and/or Temperature. *J. Chem. Phys.* **1980**, *72*, 2384−2393.

(22) Nose, S. A Unified Formulation of the Constant Temperature Molecular Dynamics Methods. *J. Chem. Phys.* **1984**, *81*, 511−519.

(23) Tuckerman, M. E. *Statistical Mechanics: Theory and Molecular Simulation*; Oxford University Press: New York, 2010.

(24) Shibuta, Y.; Suzuki, T. A Molecular Dynamics Study of Cooling Rate during Solidification of Metal Particles. *Chem. Phys. Lett.* **2011**, *502*, 82−86.

(25) Allen, M. P.; Tildesley, D. J. *Computer Simulation of Liquids*; Oxford University Press: New York, 1989.

(26) Zhuo, Y.; Karplus, M.; Ball, K. D.; Berry, R. S. The Distance Fluctuation Criterion for Melting: Comparison of Square-Well and Morse Potential Models for Clusters and Homopolymers. *J. Chem. Phys.* **2002**, *116*, 2323−2329.

(27) Gezelter, J. D.; Rabani, E.; Berne, B. J. Can Imaginary Instantaneous Normal Mode Frequencies Predict Barriers to Self-Diffusion? *J. Chem. Phys.* **1997**, *107*, 4618−4627.

(28) Daw, M. S.; Baskes, M. I. Embedded-Atom Method: Derivation and Application to Impurities, Surfaces, and Other Defects in Metals. *Phys. Rev. B* **1984**, *29*, 6443−6453.

(29) Cleri, F.; Rosato, V. Tight-Binding Potentials for Transition Metals and Alloys. *Phys. Rev. B* **1993**, *48*, 22−33.

(30) Krissinel, E. B.; Jellinek, J. 13-Atom Ni-Al Alloy Clusters: Structures and Dynamics. *Int. J. Quantum Chem.* **1997**, *62*, 185−197.

(31) Delogu, F. Demixing Phenomena in NiAl Nanometer-Sized Particles. *Nanotechnology* **2007**, *18*, 065708.

(32) Kittel, C. *Introduction to Solid State Physics*; Wiley: New York, 1966.

(33) Brandes, E. A.; Brook, G. B. *Smithells Metals Reference Handbook*; Butterworth-Heinemann: Oxford, U.K., 1992.

(34) Kubaschewski, O.; Alcock, C. B.; Spencer, P. J. *Materials Thermochemistry*; Pergamon Press: Oxford, U.K., 1993.

(35) Puri, P.; Yang, V. Effect of Voids and Pressure on Melting of Nano-Particulate and Bulk Aluminum. *J. Nanopart. Res.* **2009**, *11*, 1117−1127.

(36) Mei, Q. S.; Lu, K. Melting and Superheating of Crystalline Solids: From Bulk to Nanocrystals. *Prog. Mater. Sci.* **2007**, *52*, 1175−1262.

(37) Qi, Y.; Cagin, T.; Johnson, W. L.; Goddard, W. A. Melting and Crystallization in Ni Nanoclusters: The Mesocale Regime. *J. Chem. Phys.* **2001**, *115*, 385−394.

(38) Eckert, J.; Holzer, J. C.; Ahn, C. C.; Fu, Z.; Johnson, W. L. Melting Behavior of Nanocrystalline Aluminum Powders. *Nanostruct. Mater.* **1993**, *2*, 407−413.

(39) Lai, S. L.; Carlsoon, J. R. A.; Allen, L. H. Melting Point Depression of Al Clusters Generated during the Early Stages of Film Growth: Nanocalorimetry Measurements. *Appl. Phys. Lett.* **1998**, *72*, 1098−1100.

(40) Levitas, V. I.; Samani, K. Size and Mechanics Effects in Surface-Induced Melting of Nanoparticles. *Nat. Commun.* **2011**, *2*, 284.

(41) Levitas, V. I.; Samani, K. Coherent Solid/Liquid Interface with Stress Relaxation in a Phase-Field Approach to the Melting/Solidification Transition. *Phys. Rev. B* **2011**, *84*, 140103.

(42) Luo, S. N.; Ahrens, T. J. Superheating Systematics of Crystalline Solids. *Appl. Phys. Lett.* **2003**, *82*, 1836−1838.

(43) Daeges, J.; Gleiter, H.; Perepezko, J. H. Superheating of Metal Crystals. *Phys. Lett. A* **1986**, *119*, 79−82.

(44) Zhong, J.; Zhang, L. H.; Jin, Z. H.; Sui, M. L.; Lu, K. Superheating of Ag Nanoparticles Embedded in Ni Matrix. *Acta Mater.* **2001**, *49*, 2897−2904.

(45) Mei, Q. S.; Wang, S. C.; Cong, H. T.; Jin, Z. H.; Lu, K. Pressure-Induced Superheating of Al Nanoparticles Encapsulated in Al_2O_3 Shells Without Epitaxial Interface. *Acta Mater.* **2005**, *53*, 1059−1066.

(46) Sheng, H. W.; Ren, G.; Peng, L. M.; Hu, Z. Q.; Lu, K. Superheating and Melting-Point Depression of Pb Nanoparticles Embedded in Al Matrices. *Philos. Mag. Lett.* **1996**, *73*, 179−186.

(47) Lu, K.; Jin, Z. H. Melting and Superheating of Low-Dimensional Materials. *Curr. Opin. Solid State Mater. Sci.* **2001**, *5*, 39−44.

(48) Jin, Z. H.; Sheng, H. W.; Lu, K. Melting of Pb Clusters Without Free Surfaces. *Phys. Rev. B.* **1999**, *60*, 141−149.

(49) Hu, R.; Nash, P. The Enthalpy of Formation of NiAl. *J. Mater. Sci.* **2005**, *40*, 1067−1069.

(50) Alexander, C. A.; Ogden, J. S.; Risser, S. M.; Wood, V. E. Thermodynamic Characterization of NiAl. *J. Chem. Thermodyn.* **2009**, *41*, 610−616.

(51) Massalski, T. B. *Binary Phase Diagrams*; ASM International: Materials Park, OH, 1992.

(52) Liu, W.; Dupont, J. N. In-Situ Reactive Processing of Nickel Aluminides by Laser-Engineered Net Shaping. *Metall. Mater. Trans. A* **2003**, *34*, 2633−2641.

(53) Henz, B. J. *Molecular Dynamics Studies of Metallic Nanoparticles*. Ph.D. Thesis, University of Maryland, 2009.

(54) Levitas, V. I. Burn Time of Aluminum Nanoparticles: Strong Effect of the Heating Rate and Melt Dispersion Mechanism. *Combust. Flame* **2009**, *156*, 543−546.

(55) Levitas, V. I.; Pantoya, M.; Chauhan, G.; Rivero, L. Effect of the Alumina Shell on the Melting Temperature Depression for Aluminum Nanoparticles. *J. Phys. Chem. C* **2009**, *113*, 14088−14096.

(56) Sun, J.; Simon, S. L. The Melting Behavior of Aluminum Nanoparticles. *Thermochim. Acta* **2007**, *453*, 32−40.